

Spin-Polarized Tunneling through Chemical Vapor Deposited Multilayer Molybdenum Disulfide

Andre Dankert^{1†}, Parham Pashaei¹, M. Venkata Kamalakar^{1,2}, Anand P.S. Gaur³, Satyaprakash Sahoo^{3,4}, Ivan Rungger^{5,6}, Awadhesh Narayan^{6,7}, Kapildeb Dolui^{5,8}, Anamul Hoque¹, Michel P. de Jong⁹, Ram S. Katiyar³, Stefano Sanvito⁶, Saroj P. Dash^{1*}

¹Department of Microtechnology and Nanoscience, Chalmers University of Technology, SE-41296, Göteborg, Sweden.

²Department of Physics and Astronomy, Uppsala University, Box 516, 75120, Uppsala, Sweden

³Department of Physics and Institute for Functional Nanomaterials, University of Puerto Rico, San Juan, PR 00931, USA.

⁴Institute of Physics, Bhubaneswar, Odisha 751005, India.

⁵School of Physics, AMBER and CRANN Institute, Trinity College, Dublin 2, Ireland.

⁶National Physical Laboratory, Teddington, TW11 0LW, United Kingdom

⁷Department of Physics, University of Illinois at Urbana-Champaign, Urbana, Illinois 61801, USA

⁸Department of Physics and Astronomy, University of Delaware, Newark, Delaware 19716-2570, USA

⁹MESA⁺ Institute for Nanotechnology University of Twente 7500 AE Enschede, the Netherlands

Email: †andre.dankert@chalmers.se; *saroj.dash@chalmers.se

Abstract

The two-dimensional (2D) semiconductor molybdenum disulfide (MoS₂) has attracted widespread attention for its extraordinary electrical, optical, spin and valley related properties. Here, we report on spin polarized tunneling through chemical vapor deposited (CVD) multilayer MoS₂ (~7 nm) at room temperature in a vertically fabricated spin-valve device. A tunnel magnetoresistance (TMR) of 0.5 – 2 % has been observed, corresponding to spin polarization of 5 - 10 % in the measured temperature range of 300 – 75 K. First principles calculations for ideal junctions results in a tunnel magnetoresistance up to 8 %, and a spin polarization of 26 %. The detailed measurements at different temperatures and bias voltages, and density functional theory calculations provide information about spin transport mechanisms in vertical multilayer MoS₂ spin-valve devices. These findings form a platform for exploring spin functionalities in 2D semiconductors and understanding the basic phenomenon that control their performance.

Key words: Spin polarized tunneling, MoS₂, 2D semiconductor, Multilayer, Tunnel Magnetoresistance, Density functional theory

Spintronics is an emerging field for “beyond-CMOS” technology, where information is carried by spin instead of charge.¹ One of the primary challenges in this field is to discover novel semiconductor materials with functional spintronics properties.^{2,3,4} Two dimensional (2D) crystals offer a unique potential for spintronic devices due to remarkable properties such as long spin-coherence lengths,^{5,6} spin-polarized tunneling,^{7,8} high spin-orbit coupling (SOC)⁹ and spin-momentum locking.^{10,11} Recently, long spin coherence length in graphene has been achieved, due to its low SOC strengths and high mobility.^{6,12,13} At the same time, atomically thin molybdenum disulfide (MoS₂) has emerged as a promising semiconducting 2D crystal, demonstrating novel electronic, optoelectronic and spintronic properties. In monolayer MoS₂, the lack of inversion symmetry coupled to the high spin-orbit interaction leads to a unique spin and valley polarization.¹⁴ Recently, nanosecond electron spin lifetimes have been observed in monolayer MoS₂ at low temperatures, by using optical Kerr spectroscopy experiments.¹⁵ However, electrical realization of lateral spin transport in a MoS₂ channel remain challenging.¹⁶

The investigation of spin transport in a vertical magnetic tunnel junction (MTJ) is an interesting approach, where the transport channel is defined by a few nanometer-thick MoS₂ spacer sandwiched between two ferromagnetic (FM) electrodes. Employing such MTJs, a unique spin filtering effect was theoretically predicted for some 2D materials and first observed in graphene/graphite based devices.^{17,18,19,20} Beyond graphene, it is interesting to investigate whether similar spin filtering effects may be observed for MTJs based on insulating or semiconducting 2D crystals. Recently, insulating hexagonal boron nitride (h-BN) tunnel barriers have been used showing excellent spin polarized tunneling and filtering properties.^{21,22,7,8} Since h-BN binds little to the metallic surfaces, one may wish to fabricate MTJs with other layered compounds likely to be more reactive with the magnetic electrodes. This is for instance the case of MoS₂, since it was predicted that semiconducting multilayer MoS₂ junctions can exhibit a large TMR up to 300% in the tunneling regime.²³ Recently, *ab initio* calculations and experiments have shown that monolayer MoS₂ and WS₂ MTJs are metallic due to strong coupling between the Fe and the S atoms at the interface, showing a magnetoresistance of $\sim 0.5\%$.^{24,25,26} However, MTJs incorporating multilayer MoS₂ with semiconducting properties are expected to show enhanced performance. Such multilayered MoS₂ MTJs and room temperature operation have not been realized experimentally so far. Moreover, the possibility of using large scale multilayer MoS₂ can further enhance the impact of such devices for practical applications.

Considering the potential impact of 2D semiconductor MTJs, here we report on spin polarized tunneling through a CVD grown multilayer MoS₂ in a spin-valve structure, measuring a tunnel magnetoresistance (TMR) up to room temperature. Specifically, we have employed vertical spin-valve devices, with 7 nm thick multilayer MoS₂ sandwiched between two FM electrodes. A TMR up to 2 % is observed when the magnetic alignment of the two electrodes is switched from

parallel to anti-parallel due to the transmission of spin polarized electrons through the multilayer MoS₂ spacer. By combining bias and temperature dependent TMR measurements with density functional theory calculations, we bring out the detailed information about the spin polarization at the interfaces and the spin transport process through the multilayer MoS₂ junctions.

RESULTS AND DISCUSSION

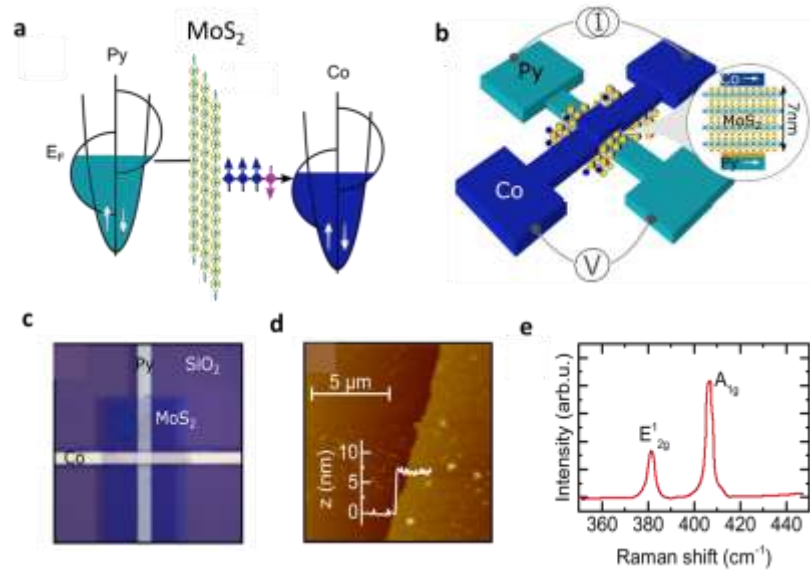


Figure 1. Multilayer MoS₂ tunnel magnetoresistance device. **a**, Spin-dependent tunneling in magnetic tunnel junctions with multilayer MoS₂ barrier. **b**, Schematic representation of the multilayer MoS₂ vertical device with ferromagnetic contacts and MoS₂ spacer. The measurement scheme is shown with four-probe cross bar geometry. **c**, Optical microscope image of a fabricated device consisting of large area CVD grown multilayer MoS₂ junction of 7 nm thickness and ferromagnetic Co and Ni₈₀Fe₂₀ (Py)/AlO_x (0.8 nm) contacts as top and bottom electrodes respectively. The active junction area is 5 × 20 μm². **d**, Atomic force microscope scan of 7 nm CVD MoS₂ on SiO₂/Si substrate. **e**, Raman spectra of 7 nm CVD MoS₂ measured at room temperature.

Tunneling magnetoresistance (TMR) is a consequence of the spin-dependent tunneling in magnetic tunnel junctions with MoS₂ barrier as shown in Fig. 1a. The device geometry shown in Fig 1b incorporates a 7nm-thick MoS₂ layer sandwiched between two FMs in a vertical structure. Specifically, the devices consist of a Ni₈₀Fe₂₀ (30 nm)/AlO_x(0.8nm)/MoS₂(7nm)/Co(50 nm) stack, fabricated using photo-lithography, metal evaporation and 2D layer transfer techniques (see Methods). The thin AlO_x layer was prepared by Al evaporation and a natural oxidation. This AlO_x layer is expected to protect the bottom Ni₈₀Fe₂₀ electrode from oxidation and acts as a leaky tunnel barrier.²⁷ An optical microscope image of a fabricated MoS₂ vertical device and the

measurement scheme is shown in Fig 1 c. The multi-layer MoS₂ chosen in our devices is grown over a large area on a SiO₂/Si substrate by CVD.²⁸ The thickness of the MoS₂ layer is determined to be 7 nm by AFM measurement as shown in Fig. 1d, which corresponds to around 10 monolayers (1 monolayer around 6.5 Å). Figure 1e shows the Raman spectrum of a MoS₂ film displaying the two Raman active modes at ~384 cm⁻¹(E_{2g}¹) and ~407 cm⁻¹ (A_{1g}) at room temperature.

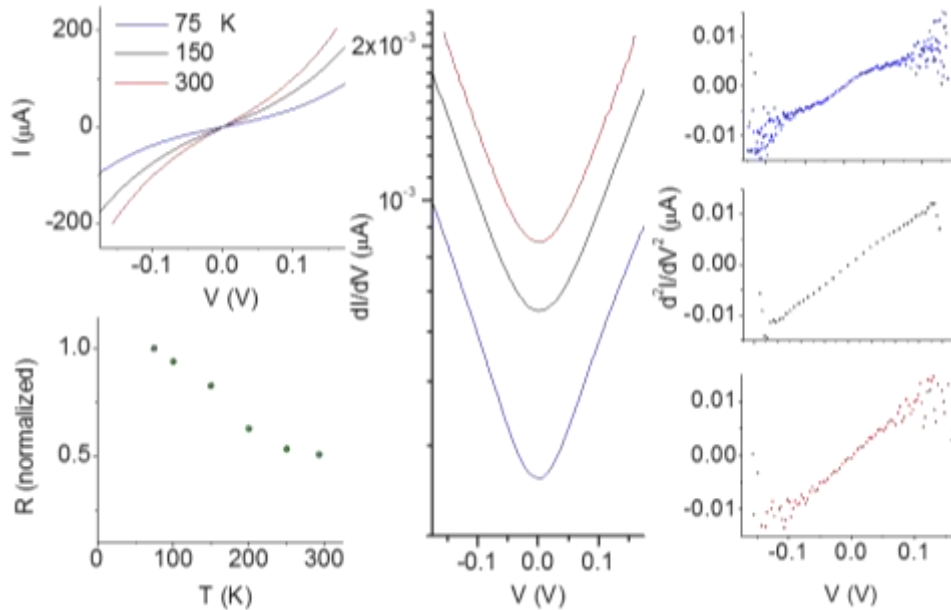


Figure 2. Electrical characterization of multilayer MoS₂ vertical devices. **a**, Current-voltage (I - V) characteristics of the junction at different temperatures. **b**, Temperature dependence of MoS₂ junction resistance (normalized) at bias voltage of 5 mV. **c**, The resistance versus bias voltage curve of the junction at temperatures of 75 K and 300 K.

The electrical transport properties of our junctions are measured in a four-terminal geometry as displayed in Fig. 1b. We observe increasingly nonlinear current-voltage (I - V) characteristics of the junction at lower temperatures (Fig. 2a). Figure 2b displays the normalized junction resistance ($R=V/I$) as a function of temperature (T), where the R value doubles when cooling down from 300 to 75 K. Such a large variation is expected due to the presence of a MoS₂ semiconducting barrier in the junction, whereas insulating Al₂O₃ barriers usually show an increase in R of 10-20% in the same range.²⁷ The strong temperature dependence can be attributed to inelastic tunneling or gap-state assisted tunneling through the MoS₂ layers.²⁹ The resistance versus bias voltage curves at both high and low temperature are quasi-symmetric as shown in Fig. 2c, signifying a deviation from a rectangular potential barrier. Considering different barrier heights for AlO_x and MoS₂, it is reasonable to assume that the overall barrier is

asymmetric. This is important for junctions made of multilayer MoS₂, which has a small band gap of only ~ 1.2 eV. The junctions are also found to be quite stable up to an applied bias of 50 mV and also do not exhibit any zero bias anomaly, suggesting the absence of magnetic impurities.

The junction resistance for thick MoS₂ (7 nm) consists of both the inter-layer and intra-layer resistances. The couplings between the MoS₂ layers are expected to arise from the overlap of the electron wave functions due to the small separation between the sulfide layers, with charge screening length of ~7 nm.³⁰ This is distinctly different from the current distribution in multilayer graphene with charge screening length of only 0.6 nm.³¹ The difference arises due to the transport involving the d-electrons of MoS₂, while the p_z-orbitals are responsible in graphene. For thinner MoS₂ layers (few monolayers) a direct tunneling dominates, with the tunneling conductance exponentially decreasing with increasing the MoS₂ thickness.^{32,33,34} However, for thicker samples used in the present study, inelastic tunneling or gap-state assisted tunneling through defects in the form of S vacancies cannot be ruled out.²⁹

Next, we performed magnetoresistance measurements with 7 nm multilayer MoS₂ MTJs by applying a fixed bias current (constant current mode) while measuring the voltage drop as a function of the external in-plane magnetic field, B . The TMR across the MoS₂ junction is observed at room temperature as a difference in the resistances measured for the parallel, R_p , and antiparallel, R_{ap} , alignment of the magnetizations of the FM electrodes as shown in Fig. 3a. The well-defined resistance states R_p and R_{ap} are achieved by using different FM materials (Co and NiFe) and electrode widths on either side of the MoS₂ layer. The measured magneto voltage signal of $\Delta V = 15 \mu\text{V}$ corresponds to a $TMR = \frac{R_p - R_{ap}}{R_p} \times 100\% = 0.5\%$ at 300 K. We estimate the spin polarization of the contacts from the Julliere relation $TMR = \frac{2P_1P_2}{1 - P_1P_2}$,^{35,36} and these turn out to be $P_1 = P_2 = 5\%$ (assuming the polarizations of Co and Ni₈₀Fe₂₀ to be the same). We would like to note that the spin polarization obtained with introduction of MoS₂ is smaller than the polarization of ferromagnetic tunnel contacts reported in literature.³⁶ This can be attributed to disorder introduced at the interfaces during the wet transfer process of the CVD MoS₂ layer onto the ferromagnetic electrode. It has also to be noted that the spin transport process is very sensitive to defect assisted tunneling (i.e. multi-step tunneling) through MoS₂ and can significantly affect the TMR.³⁷ This can cause additional spin flip scattering due to the presence of strong spin-orbit coupling in MoS₂.³⁸ As predicted theoretically, the spin polarization is expected to be higher with development of all in-situ method for preparation of good quality MoS₂ layers and ferromagnetic tunnel contacts. However, our effort to integrate ferromagnetic tunnel junction to CVD MoS₂ in an ex-situ fabrication process shows promising results with a TMR up to room temperature.

Even though the observation of a TMR offers evidence for spin-polarized transport, a careful investigation of the bias and temperature dependence is essential for physical understanding of the phenomenon. The applications of negative and positive bias voltages correspond to a spin transport through the MoS₂ from Ni₈₀Fe₂₀ to Co and Co to Ni₈₀Fe₂₀ respectively. The bias dependence of the TMR signal changes sign with reversing bias polarity (shown in Fig. 3a). The bias dependence of the absolute value of TMR at room temperature measured at different voltages across the junction is shown in Fig. 3b. We observe a decrease of the TMR at higher bias voltages with a maximum around zero bias voltage. Such behavior can be attributed to the excitation of magnons, to band bending and possibly to the involvement of interface states at high voltages, as also observed in other material systems.³⁹ The bias dependence is also found to be asymmetric with polarity, decreasing much faster in the negative than the positive bias range. This behavior can be due to asymmetric barrier interfaces (Co/MoS₂ and Ni₈₀Fe₂₀/AlO_x/MoS₂) at the two sides of the MoS₂ layer. Similar bias dependence behavior has also been observed in some cases in other magnetic tunnel junctions with inorganic and organic semiconductors,⁴⁰ and tunnel junctions with Al₂O₃, MgO and h-BN.^{41,42,22}

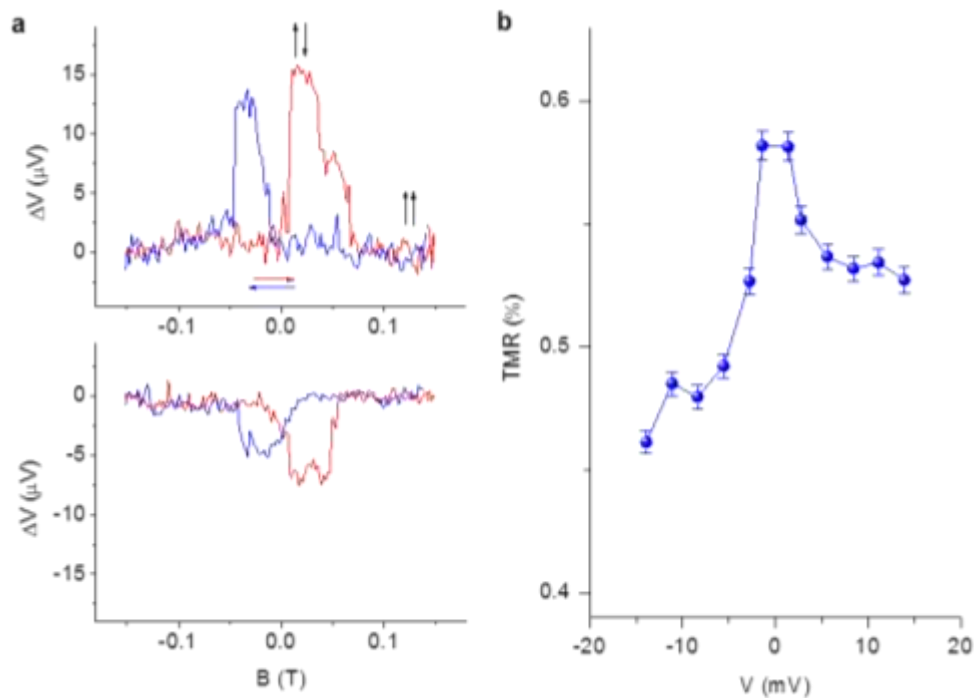


Figure 3. Spin-valve measurements in multilayer MoS₂ MTJs at room temperature. **a**, Tunnel magnetoresistance (TMR) measurements on the device with an in-plane magnetic field B_{in} for applied bias voltages of +10 mV (upper panel) and -5 mV (lower panel) at room temperature (300 K). The arrows indicate the up and down B field sweep directions. **b**, Bias dependence of TMR signal measured at 300 K.

In order to investigate the details of the spin transport process through MoS₂, spin-valve measurements were performed at different temperatures. The TMR shows an overall increase up

to 2% at 75 K, corresponding to a spin polarization of 10% (as extracted from Julliere's formula³⁵). Figure 4a shows the TMR at 75 K and 300 K and the normalized TMR as a function of temperature is plotted in Fig. 4b. We model the observed decrease in TMR with increase in temperature by considering the spin polarization to have the same temperature dependence as surface magnetization, which is described by the spin wave excitation model with $T^{3/2}$ dependence.⁴³ We observe a faster decrease of the TMR at higher temperatures, in comparison to the expected moderate decrease. Such behavior can be attributed to the low bandgap of ~ 1.2 eV and correspondingly low barrier height of the multilayer MoS₂ barrier.

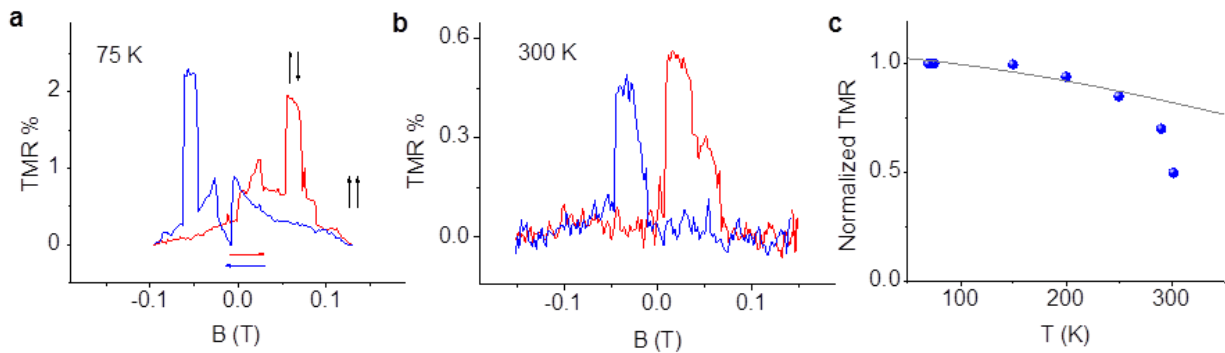


Figure 4. Temperature dependence of TMR in multilayer MoS₂ MTJ. **a**, Tunnel magnetoresistance (TMR) measurements at 75 K. **b**, TMR measured at 300 K. The arrows indicate the up and down B field sweep directions. **c**, Temperature dependence of TMR signal (normalized). The fitting represents the temperature dependence of $TMR \propto 1 - \alpha T^{3/2}$.

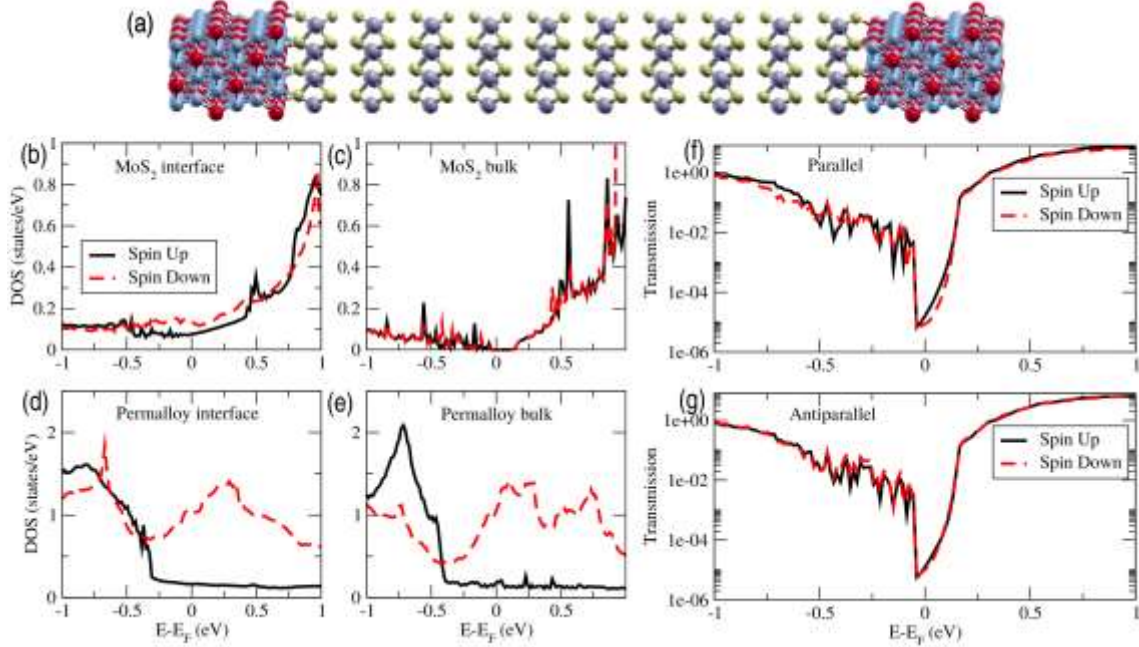


Figure 5. Theoretical results for a permalloy/MoS₂/permalloy junction. (a) Junction setup for transport calculations with ten layers of MoS₂, corresponding to a barrier thickness of about 6.4 nm, sandwiched between semi-infinite permalloy (Ni₈₀Fe₂₀) electrodes. Density of states (DOS) as a function of energy for the (b) interface MoS₂ layer, (c) MoS₂ layer in the bulk of the spacer, (d) interface permalloy layer and (e) bulk permalloy. Spin resolved transmission in (f) for parallel and (g) antiparallel configurations of the junction.

In order to further understand the transport properties of the devices, we have carried out density functional theory based transport calculations for an ideal, defect-free junction (see Computational Methods for details). The setup for our computations is shown in Fig. 5(a) for a junction made of ten MoS₂ layers sandwiched between two semi-infinite permalloy (Ni₈₀Fe₂₀) electrodes. Note that we use permalloy for both electrodes, which is a reasonable approximation since the Co density of states (DOS) is rather similar to the one of permalloy.⁴⁴ The use of an approximately symmetric setup is also justified by the rather small asymmetry found in the experimental *I-V* and TMR-*V* curves. The spin resolved DOS projected onto different layers of the junction are shown in Fig. 5(b)-(e). We find that the MoS₂ interface layer becomes metallic due to a strong hybridization with permalloy, similar to what has been found for single layer MoS₂.²⁴ In contrast, as one moves into the bulk of the spacer, a gap reminiscent of pristine MoS₂ emerges. Notably, the DOS at the Fermi level of the interface MoS₂ layer becomes spin polarized, which indicates spin injection into MoS₂. Considering the first MoS₂ layer as the effective metallic interface layer, we find the theoretical upper limit to the efficiency for spin injection in this junction, as $\eta = (DOS_{\downarrow} - DOS_{\uparrow}) / (DOS_{\downarrow} + DOS_{\uparrow}) \sim 26\%$. This number is significantly smaller than the value in the bulk permalloy (73%) and at the permalloy interface layer (76%).

The spin resolved transmission as a function of energy for the parallel and antiparallel configurations is plotted in Fig. 5(f) and (g), respectively. At the Fermi level, we find $MR = (T_{\text{parallel}} - T_{\text{antiparallel}}) / T_{\text{antiparallel}} \sim 8\%$. This MR value, under ballistic transport conditions for an ideal tunnel junction, should be considered as an upper limit to the MR for devices with permalloy

electrodes. The presence of defects in MoS₂, as well as inelastic scattering processes can reduce the spin polarization of the current, thereby reducing the measured magnetoresistance down to the experimentally measured values. Note that the MR obtained here is rather similar to that of a single MoS₂ layer with permalloy electrodes,²⁴ and significantly lower than what was predicted in a previous study for MoS₂ junctions with Fe electrodes,²³ where it was found to increase with MoS₂ thickness. The origin of the reduced MR found here lies in the reduced polarization and spin filtering induced by the permalloy electrodes when compared to Fe electrodes, which also have a better lattice match with MoS₂. This observation also shows that the choice of electrode materials and lattice matching are crucial factors in obtaining high magnetoresistance in MoS₂ based tunnel junctions.

CONCLUSION

In summary, we have demonstrated spin-polarized tunneling in multilayer MoS₂ at room temperature in a vertical spin-valve device. The spin-transport through 7 nm of MoS₂ produces a TMR of 0.5% at room temperature, which shows enhancement up to 2% at 75 K, corresponding to an increase of spin polarization from 5 to 10%. Our density functional theory based transport calculations for ideal spin valves provide an upper limit to the TMR to be 8%, while the maximum spin polarization is obtained to be 26%. The theoretical results also show that interfaces without epitaxial growth generally lead to rather low MR ratios when compared to junctions with better lattice match across the layers. The lower experimentally obtained spin polarization possibly can be attributed to interface contamination during transfer process, defect assisted tunneling and spin flip scattering due to spin-orbit coupling in MoS₂. These results on vertical spin-transport in large area multilayer MoS₂ reveal useful information needed for the development of 2D semiconductor materials and their heterostructures for spintronic devices and will open the path for the observation of novel spintronic effects. One particularly interesting new topic would be to investigate spintronic devices based on 2D material heterostructures by integrating the MoS₂ layers into graphene spin transport channels⁴.

EXPERIMENTAL METHODS

Materials growth and characterization. We fabricated the MoS₂/ferromagnetic metal heterostructures using MoS₂ films grown by chemical vapor deposition (CVD). The large area MoS₂ films were synthesized on SiO₂/Si substrates via CVD and sulfurization of molybdenum films at 900 °C. The film thickness was characterized in tapping mode atomic force microscopy (AFM-VEECO). Raman and photoluminescence (PL) spectroscopy were carried out using Horiba-Jobin T64000 (triple mode subtractive) micro-Raman system in backscattering configuration utilizing Argon ion laser (514.5 nm line as excitation source).

Device fabrication. Spin transport devices incorporating a multilayer MoS₂ between two FM metal electrodes in a vertical geometry are fabricated. The bottom Ni₈₀Fe₂₀ (30 nm) electrodes

are prepared on a Si/SiO₂ substrate by photolithography, electron beam evaporation and lift off methods. Before deposition of NiFe electrodes, we deposited a thin layer of Ti in order to increase adhesion of FM to the SiO₂ substrate. The bottom NiFe electrodes are capped with 0.8 nm Al and subsequently oxidized naturally to make an AlO_x layer, which should protect the bottom ferromagnet NiFe from oxidation and contamination during transfer of MoS₂.

The large area MoS₂ films grown on SiO₂ substrate were first covered with PMMA layer and then released from the substrate by etching in KOH. After a de-ionized (DI) water rinse, the MoS₂/PMMA layer was transferred onto the bottom Ni₈₀Fe₂₀ electrodes. After drying the chip in an ambient environment, we annealed it at 150 °C for 10 min. It has been observed that this annealing step improved adhesion of MoS₂ with the bottom Ni₈₀Fe₂₀ electrode. The chip was then cleaned with acetone to remove the PMMA. The active device areas of MoS₂ layer were patterned by lithography and Ar ion beam etching with SIMS etch stop technique. The top Co (65 nm) electrodes and capping Au (20 nm) layer were prepared by photolithography, electron beam evaporation and lift off techniques in a cross-bar geometry. The final device consists of junctions with Ni₈₀Fe₂₀ (30 nm)/AlO_x (0.8 nm)/MoS₂ (7 nm)/Co (65 nm) heterostructures.

Computational Methods. Ab initio transport calculations were performed using the *Smeagol* package,^{45,46,47}. The code interfaces non-equilibrium Green's function method for transport with density functional theory, as implemented in SIESTA code.⁴⁸ Norm conserving pseudopotentials were used to replace the core electrons and a double ζ polarized basis set was employed, along with a mesh cutoff of 300 Rydberg. Local density approximation to the exchange correlation functional was used.⁴⁹ An in-plane supercell of dimensions 14.37 Å x 8.29 Å was constructed, with the total length of the scattering region along the transport direction being 82.65 Å. Periodic boundary conditions were implemented perpendicular to the transport direction, with a 2x4 k -point mesh sampling used for the self-consistent calculations. Transmission coefficients and densities of states were obtained for the so converged charge density by integrating over a denser 10x20 k -point grid.

Acknowledgement

S. Dash acknowledges financial support from the NanoAoA, Swedish Research Council, EU Graphene Flagship, EU FlagEra. R. Katiyar acknowledges financial support from DOE (Grant No. DEG02-ER46526) and stipend to A. Gaur. S. Sahoo acknowledges receiving financial support as PDF through NSF Grant #EPS-01002410. S. Sanvito thanks Science Foundation Ireland (grant No. 14/IA/2624) for financial support. "I.R. thanks the European Union for financial support through the FP7 project ACMOL (Grant agreement number 618082).

References

- (1) Žutić, I.; Fabian, J.; Sarma, S. Das. Spintronics: Fundamentals and Applications. *Reviews of Modern Physics*, 2004, 76, 323–410.
- (2) Awschalom, D. D.; Flatté, M. E. Challenges for Semiconductor Spintronics. *Nature Physics*, 2007, 3, 153–159.
- (3) Dash, S. P.; Sharma, S.; Patel, R. S.; de Jong, M. P.; Jansen, R. Electrical Creation of Spin Polarization in Silicon at Room Temperature. *Nature* **2009**, 462, 491–494.
- (4) Roche, S.; Åkerman, J.; Beschoten, B.; Charlier, J.-C.; Chshiev, M.; Prasad Dash, S.; Dlubak, B.; Fabian, J.; Fert, A.; Guimarães, M.; *et al.* Graphene Spintronics: The European Flagship Perspective. *2D Mater.* **2015**, 2, 30202.
- (5) Tombros, N.; Jozsa, C.; Popinciuc, M.; Jonkman, H. T.; van Wees, B. J. Electronic Spin Transport and Spin Precession in Single Graphene Layers at Room Temperature. *Nature* **2007**, 448, 571–574.
- (6) Kamalakar, V. M.; Groenveld, C.; Dankert, A.; Dash, S. P. Long Distance Spin Communication in Chemical Vapour Deposited Graphene. *Nat. Commun.* **2015**, 6, 6766.
- (7) Kamalakar, M. V.; Dankert, A.; Bergsten, J.; Ive, T.; Dash, S. P. Enhanced Tunnel Spin Injection into Graphene Using Chemical Vapor Deposited Hexagonal Boron Nitride. *Sci. Rep.* **2014**, 4, 6146.
- (8) Kamalakar, M. V.; Dankert, A.; Kelly, P. J.; Dash, S. P. Inversion of Spin Signal and Spin Filtering in Ferromagnet|Hexagonal Boron Nitride-Graphene van Der Waals Heterostructures. *Sci. Rep.* **2016**, 6, 21168.
- (9) Gong, Z.; Liu, G.-B.; Yu, H.; Xiao, D.; Cui, X.; Xu, X.; Yao, W. Magnetoelectric Effects and Valley-Controlled Spin Quantum Gates in Transition Metal Dichalcogenide Bilayers. *Nat. Commun.* **2013**, 4, 2053.
- (10) Li, C. H.; van 't Erve, O. M. J.; Robinson, J. T.; Liu, Y.; Li, L.; Jonker, B. T. Electrical Detection of Charge-Current-Induced Spin Polarization due to Spin-Momentum Locking in Bi₂Se₃. *Nat. Nanotechnol.* **2014**, 9, 218–224.
- (11) Dankert, A.; Geurs, J.; Kamalakar, M. V.; Charpentier, S.; Dash, S. P. Room Temperature Electrical Detection of Spin Polarized Currents in Topological Insulators. *Nano Lett.* **2015**, 15, 7976–7981.
- (12) Drögeler, M.; Franzen, C.; Volmer, F.; Pohlmann, T.; Banszerus, L.; Wolter, M.; Watanabe, K.; Taniguchi, T.; Stampfer, C.; Beschoten, B. Spin Lifetimes Exceeding 12 Ns in Graphene Nonlocal Spin Valve Devices. *Nano Lett.* **2016**, acs.nanolett.6b00497.
- (13) Ingla-Aynés, J.; Guimarães, M. H. D.; Meijerink, R. J.; Zomer, P. J.; Van Wees, B. J. 24- μ M Spin Relaxation Length in Boron Nitride Encapsulated Bilayer Graphene. *Phys. Rev. B - Condens. Matter Mater. Phys.* **2015**, 92.
- (14) Xu, X.; Yao, W.; Xiao, D.; Heinz, T. F. Spin and Pseudospins in Layered Transition Metal Dichalcogenides. *Nat. Phys.* **2014**, 10, 343–350.
- (15) Yang, L.; Sinitsyn, N. a.; Chen, W.; Yuan, J.; Zhang, J.; Lou, J.; Crooker, S. A. Long-Lived Nanosecond Spin Relaxation and Spin Coherence of Electrons in Monolayer MoS₂ and WS₂. *Nat. Phys.* **2015**, 1–6.

- (16) Dankert, A.; Langouche, L.; Kamalakar, M. V.; Dash, S. P. High-Performance Molybdenum Disulfide Field-Effect Transistors with Spin Tunnel Contacts. *ACS Nano* **2014**, *8*, 476–482.
- (17) Karpan, V. M.; Giovannetti, G.; Khomyakov, P. A.; Talanana, M.; Starikov, A. A.; Zwierzycki, M.; Van Den Brink, J.; Brocks, G.; Kelly, P. J. Graphite and Graphene as Perfect Spin Filters. *Phys. Rev. Lett.* **2007**, *99*.
- (18) Cobas, E.; Friedman, A. L.; Van'T Erve, O. M. J.; Robinson, J. T.; Jonker, B. T. Graphene as a Tunnel Barrier: Graphene-Based Magnetic Tunnel Junctions. *Nano Lett.* **2012**, *12*, 3000–3004.
- (19) Martin, M. B.; Dlubak, B.; Weatherup, R. S.; Yang, H.; Deranlot, C.; Bouzehouane, K.; Petroff, F.; Anane, A.; Hofmann, S.; Robertson, J.; *et al.* Sub-Nanometer Atomic Layer Deposition for Spintronics in Magnetic Tunnel Junctions Based on Graphene Spin-Filtering Membranes. *ACS Nano* **2014**, *8*, 7890–7895.
- (20) Iqbal, M. Z.; Iqbal, M. W.; Lee, J. H.; Kim, Y. S.; Chun, S. H.; Eom, J. Spin Valve Effect of NiFe/graphene/NiFe Junctions. *Nano Res.* **2013**, *6*, 373–380.
- (21) Karpan, V. M.; Khomyakov, P. A.; Giovannetti, G.; Starikov, A. A.; Kelly, P. J. Ni(111)|graphene|h-BN Junctions as Ideal Spin Injectors. *Phys. Rev. B - Condens. Matter Mater. Phys.* **2011**, *84*.
- (22) Dankert, A.; Venkata Kamalakar, M.; Wajid, A.; Patel, R. S.; Dash, S. P. Tunnel Magnetoresistance with Atomically Thin Two-Dimensional Hexagonal Boron Nitride Barriers. *Nano Res.* **2015**, *8*, 1357–1364.
- (23) Dolui, K.; Narayan, A.; Rungger, I.; Sanvito, S. Efficient Spin Injection and Giant Magnetoresistance in Fe/MoS₂/Fe Junctions. *Phys. Rev. B - Condens. Matter Mater. Phys.* **2014**, *90*.
- (24) Wang, W.; Narayan, A.; Tang, L.; Dolui, K.; Liu, Y.; Yuan, X.; Jin, Y.; Wu, Y.; Rungger, I.; Sanvito, S.; *et al.* Spin-Valve Effect in NiFe/MoS₂/NiFe Junctions. *Nano Lett.* **2015**, *15*, 5261–5267.
- (25) Wu, H.-C.; Coileáin, C. Ó.; Abid, M.; Mauit, O.; Syrlybekov, A.; Khalid, A.; Xu, H.; Gatensby, R.; Jing Wang, J.; Liu, H.; *et al.* Spin-Dependent Transport Properties of Fe₃O₄/MoS₂/Fe₃O₄ Junctions. *Sci. Rep.* **2015**, *5*, 15984.
- (26) Iqbal, M. Z.; Iqbal, M. W.; Siddique, S.; Khan, M. F.; Ramay, S. M. Room Temperature Spin Valve Effect in NiFe/WS₂/Co Junctions. *Sci. Rep.* **2016**, *6*, 21038.
- (27) Santos, T. S.; Lee, J. S.; Migdal, P.; Lekshmi, I. C.; Satpati, B.; Moodera, J. S. Room-Temperature Tunnel Magnetoresistance and Spin-Polarized Tunneling through an Organic Semiconductor Barrier. *Phys. Rev. Lett.* **2007**, *98*.
- (28) Gaur, A. P. S.; Sahoo, S.; Ahmadi, M.; Dash, S. P.; Guinel, M. J. F.; Katiyar, R. S. Surface Energy Engineering for Tunable Wettability through Controlled Synthesis of MoS₂. *Nano Lett.* **2014**, *14*, 4314–4321.
- (29) Ahmed, F.; Choi, M. S.; Liu, X.; Yoo, W. J. Carrier Transport at the Metal-MoS₂ Interface. *Nanoscale* **2015**, *7*, 9222–9228.
- (30) Das, S.; Appenzeller, J. Where Does the Current Flow in Two-Dimensional Layered Systems? *Nano Lett.* **2013**, *13*, 3396–3402.
- (31) Sui, Y.; Appenzeller, J. Screening and Interlayer Coupling in Multilayer Graphene Field-Effect Transistors. *Nano Lett.* **2009**, *9*, 2973–2977.
- (32) Yu, W. J.; Li, Z.; Zhou, H.; Chen, Y.; Wang, Y.; Huang, Y.; Duan, X. Vertically Stacked Multi-Heterostructures of Layered Materials for Logic Transistors and Complementary Inverters. *Nat.*

- Mater.* **2013**, *12*, 246–252.
- (33) Moriya, R.; Yamaguchi, T.; Inoue, Y.; Sata, Y.; Morikawa, S.; Masubuchi, S.; Machida, T. Influence of the Density of States of Graphene on the Transport Properties of graphene/MoS₂/metal Vertical Field-Effect Transistors. *Appl. Phys. Lett.* **2015**, *106*, 223103.
- (34) Sata, Y.; Moriya, R.; Morikawa, S.; Yabuki, N.; Masubuchi, S.; Machida, T. Electric Field Modulation of Schottky Barrier Height in graphene/MoSe₂ van Der Waals Heterointerface. *Appl. Phys. Lett.* **2015**, *107*, 23109.
- (35) Julliere, M. Tunneling between Ferromagnetic Films. *Phys. Lett. A* **1975**, *54*, 225–226.
- (36) Moodera, J. S.; Kinder, L. R.; Wong, T. M.; Meservey, R. Large Magnetoresistance at Room Temperature in Ferromagnetic Thin Film Tunnel Junctions. *Phys. Rev. Lett.* **1995**, *74*, 3273–3276.
- (37) Tran, T. L. A.; Le, T. Q.; Sanderink, J. G. M.; Van Der Wiel, W. G.; De Jong, M. P. The Multistep Tunneling Analogue of Conductivity Mismatch in Organic Spin Valves. *Adv. Funct. Mater.* **2012**, *22*, 1180–1189.
- (38) Xiao, D.; Liu, G. Bin; Feng, W.; Xu, X.; Yao, W. Coupled Spin and Valley Physics in Monolayers of MoS₂ and Other Group-VI Dichalcogenides. *Phys. Rev. Lett.* **2012**, *108*.
- (39) Moodera, J.; Nowak, J.; van de Veerdonk, R. Interface Magnetism and Spin Wave Scattering in Ferromagnet-Insulator-Ferromagnet Tunnel Junctions. *Phys. Rev. Lett.* **1998**, *80*, 2941–2944.
- (40) Xiong, Z. H.; Wu, D.; Vardeny, Z. V.; Shi, J. Giant Magnetoresistance in Organic Spin-Valves. *Nature* **2004**, *427*, 821–824.
- (41) Park, B. G.; Banerjee, T.; Lodder, J. C.; Jansen, R. Tunnel Spin Polarization versus Energy for Clean and Doped Al₂O₃ Barriers. *Phys. Rev. Lett.* **2007**, *99*.
- (42) Yuasa, S.; Nagahama, T.; Fukushima, A.; Suzuki, Y.; Ando, K. Giant Room-Temperature Magnetoresistance in Single-Crystal Fe/MgO/Fe Magnetic Tunnel Junctions. *Nat. Mater.* **2004**, *3*, 868–871.
- (43) Shang, C.; Nowak, J.; Jansen, R.; Moodera, J. Temperature Dependence of Magnetoresistance and Surface Magnetization in Ferromagnetic Tunnel Junctions. *Phys. Rev. B* **1998**, *58*, R2917–R2920.
- (44) Coey, J. M. D. *Magnetism and Magnetic Materials*; 2010; Vol. 12.
- (45) Rocha, A. R.; García-suárez, V. M.; Bailey, S. W.; Lambert, C. J.; Ferrer, J.; Sanvito, S. Towards Molecular Spintronics. *Nat. Mater.* **2005**, *4*, 335–339.
- (46) Rocha, A. R.; García-Suárez, V. M.; Bailey, S.; Lambert, C.; Ferrer, J.; Sanvito, S. Spin and Molecular Electronics in Atomically Generated Orbital Landscapes. *Phys. Rev. B - Condens. Matter Mater. Phys.* **2006**, *73*.
- (47) Rungger, I.; Sanvito, S. Algorithm for the Construction of Self-Energies for Electronic Transport Calculations Based on Singularity Elimination and Singular Value Decomposition. *Phys. Rev. B - Condens. Matter Mater. Phys.* **2008**, *78*.
- (48) Soler, J. M.; Artacho, E.; Gale, J. D.; Garcia, A.; Junquera, J.; Ordejon, P.; Sanchez-Portal, D. The SIESTA Method for Ab Initio Order-N Materials Simulation. *J. physics. Condens. matter* **2002**, *2745*, 22.
- (49) Ceperley, D. M.; Alder, B. J. Ground State of the Electron Gas by a Stochastic Method. *Phys. Rev. Lett.* **1980**, *45*, 566–569.

TOC graphic

